Publishing Excellence Inspiring Progress
ARISTON PUBLICATIONS
Science of Alloys and Glasses
ISSN: 3143-0732 https://aristonpubs.com/journal/science-of-alloys-and-glasses https://doi.org/10.69626/sag.2025.0179

RESEARCH ARTICLE

Evaluation of CuO Nanoparticles as Potential Gamma–Ray Shielding Materials Using EpiXS Calculations

Hend Abd-Allah [1], Atef El-Taher [2,*]

ABSTRACT: Copper oxide (CuO) nanoparticles were synthesized via a simple and cost-effective coprecipitation method and evaluated for their gamma-ray shielding potential. The radiation attenuation performance was investigated over a wide photon energy range (5 keV–15 MeV) using the EpiXS computational program. Key shielding parameters, including mass attenuation coefficient (MAC), linear attenuation coefficient (LAC), half-value layer (HVL), mean free path (MFP), effective atomic number (Zeff), and photon buildup factors, were systematically analyzed. The results reveal a pronounced energy-dependent shielding behavior. At low photon energies, dominated by the photoelectric effect, CuO nanoparticles exhibit excellent attenuation performance, achieving LAC and MAC values of 1002.13 cm^{-1} and 161.226 $cm^2 g^{-1}$ at 5 keV, respectively. With increasing photon energy, attenuation parameters decrease significantly due to the predominance of Compton scattering, followed by a slight rise in MAC values at higher energies (>1.022 MeV) attributed to pair production. The shielding efficiency is further confirmed by extremely low HVL and MFP values at low energies, indicating that minimal material thickness is sufficient for effective radiation attenuation. The effective atomic number (Zeff) of CuO nanoparticles ranges between approximately 18 and 25 across the investigated energy spectrum, reflecting favorable photon–matter interactions. Overall, the synthesized CuO nanoparticles demonstrate promising gamma-ray shielding performance, particularly in the low- and intermediate-energy regions. Owing to their facile synthesis, lightweight nature, and environmentally benign characteristics, CuO nanoparticles represent a viable alternative to conventional heavy and toxic shielding materials for radiation protection and medical physics applications.

Keywords: CuO nanoparticles, Shielding materials, Mass attenuation coefficient (MAC), Linear Attenuation Coefficient (LAC), Gamma-ray attenuation.

Received: 19 February 2025; Revised: 16 May 2025; Accepted: 30 June 2025; Published Online: 21 July 2025

1. INTRODUCTION

Today, radiation protection is a critical issue, particularly in nuclear energy, space exploration, and radiation medicine, where workers must be protected from radiation. Because X-rays and γ-rays can penetrate these two more deeply, they pose the greatest risk to public health and equipment of any high-energy photoirradiation. Shields made of appropriate materials offer the best protection, lowering the intensity of these rays and thus their harmful effects. Shielding materials can mitigate the effects of these rays by interacting with them and decreasing their output. The linear and mass attenuation coefficients are two numbers that represent the ability of the shielding material to reduce the intensity of radiation.

The most likely -ray attenuation interactions are best described by the photoelectric effect (PE), Compton scattering (CS), and pair production (PP) mechanisms [1]. Several factors must be considered when selecting an

[1] Department of Physics, Faculty of Science, Assiut University, Assiut, 71516, Egypt
[2] Physics Department, Faculty of Science, Al-Azhar University, Assiut, 71452, Egypt

* Author to whom correspondence should be addressed: atef.eltaher@gmail.com (Atef El-Taher)

© Ariston Publications 2025. All rights reserved.

appropriate shielding material and determining its thickness, including the type, intensity, and power of the radiation source, the cost-effectiveness of that material, the activity of the radioisotope, and the rate of radiation exposure. The photon energy of the rays impinging on the shield, as well as the density (ρ) and atomic weight (Z) of the shielding material, determine the likelihood of an interaction between -rays and the shield. To absorb -rays, iron and other materials are commonly used. However, these shields have some disadvantages, such as low mechanical strength, chemical resistance, heaviness, and processability. Nuclear power plants and hospital X-ray radiology are examples of nuclear activities that produce gamma rays, X-rays, and fast neutrons. investigation of new materials [2].

Recently, nanomaterials have been used in a variety of nanotechnology applications, including radiation shielding. Several nanomaterials and nanocomposites for radiation shielding against various ionising energies have been reported. As a result, several research studies have focused on gamma-ray shielding using various materials such as concrete, clay, polymers, and heavy metal oxides [3]. Several nanocomposites made of metal or metal oxide particles in the nano-dimension have recently been developed. These nanocomposites are used to improve flexibility in radiation shielding [4], comfortability [5], cost-effectiveness, light weight [6], and environmental friendliness [7- 9]. NPs are one of the key possibilities to replace Pb as one of the most preferred nanofillers in γ -ray shielding. is not hazardous in comparison to lead, and its radiation shielding qualities against γ-rays are comparable to lead [9, 10].

The developed material has potential applications in fields utilizing hazardous radiation, such as protective clothing for radiation workers, shielding for radioactive transport, and waste management. Common materials include lead, tungsten, bismuth, and cadmium, widely used in areas like radiography and security. However, lead's toxic effects raise concerns about its health and environmental impact, necessitating limits on its use. Alternatives like concrete are also common for shielding against ionizing radiation. Recent advancements have introduced nanomaterials as promising substitutes due to their advantages, including being lightweight and non-toxic. While numerous studies focus on the gamma ray shielding properties of nanomaterials, research on their efficacy against gamma and neutron radiation remains limited [11- 16]. Salisu et.al. used the WinXCOM software t for impact of CuO doping on other parameters like HVL and MFP, and concluded that doping CuO with concrete enhances gamma shielding ability. The MAC values of the samples showed a rapid decrease up to 0.12 MeV [11]. Alwesabi et al. studied the shielding properties of zinc oxide-copper oxide nanocomposites against gamma rays, and physical and structural properties were explored. The nanocomposites exhibit high shielding effectiveness against gamma rays, with attenuation coefficients ranging from 0.12 to 0.25. Their physical properties, such as density and compressive strength, are also investigated. The nanocomposites demonstrate promising structural properties, with high compressive strengths and low densities [12].

Nanomaterials have emerged as a novel replacement material for the drawbacks of lead and concrete materials used in radiation shielding as a result of extensive research in this field. Nanomaterials outperform lead and concrete because they are transparent, additive, inexpensive, lightweight, simple to manufacture, and, most importantly, have no negative health consequences. There have been numerous studies on the gamma ray shielding of nanomaterials. In contrast, studies on the gamma and neutron shielding of glass materials are uncommon. Recently, researchers and technologists have become interested in studying the various properties and parameters of nanomaterials [17-22].

The research focuses on the fabrication of CuO nanoparticles via the coprecipitation method to investigate their potential for radiation shielding applications. The study specifically examined crucial radiation shielding parameters, such as the Mass Attenuation Coefficient (MAC), Linear Attenuation Coefficient (LAC), Atomic Cross-Section (ACS), Electronic Cross-Section (ECS), and Effective Atomic Number (Z_{eff}). Key features indicating an effective shielding material are Half-Value Layer (HVL) and low Mean Free Path (MFP) values. Shielding properties were calculated using the EpiXs method.

2. EXPERIMENTAL DETAILS

2.1. Preparation of CuO nanoparticles

We prepared CuO by the coprecipitation method. CuO nanoparticles s were created by precipitation using copper nitrate (Cu $(NO_3)_2.3H_2O$) to create a 0.1 M concentration. Each precursor was first dissolved in 100 milliliters of deionized water. A 0.1 M NaOH solution was gradually added while being vigorously stirred until the pH attained 14. After obtaining black precipitates, they were periodically cleaned with deionized water and 100% ethanol until the pH reached 7. The cleaned precipitates were then dried for 16 hours at 100 °C. The precursors were then calcined for 3 hours at 500 °C.

2.2. EpiXS software

A Windows-based application software EpiXS was constructed for photon attenuation, dosimetry and shielding, and is based on EPICS2017 of ENDF/B-VIII and EPDL97 of ENDF/B-VI.8. For any user-defined material, the software interpolates data libraries between 1 keV and 100 GeV and computes partial or total cross sections (σ), mass attenuation coefficients (μ/ρ), linear attenuation coefficients (μ), mean free paths (MFP), half-value layers (HVL), effective atomic numbers (Z_{eff}), electron densities (N_{eff}), and the auxiliary parameters and buildup factors for energy absorption (EABF) and exposure (EBF) via Geometric-Progression [23].

© Ariston Publications 2025. All rights reserved.

2.3. Radiation-absorbing parameter calculation procedure

The radiation intensity (I) with absorbent material, thickness t, and radiation intensity before encountering the material have a relationship, as shown in the following equation (I_o).

$$I = Ioe^{-\mu x} \quad (1)$$

Where μ is the coefficient of linear radiation attenuation. The Mass Attenuation Coefficient (MAC) is a straightforward term that describes a shielding material's ability to reduce gamma radiation by dividing it by its specific gravity. The samples' MAC values were determined using the [24–16]:

$$MAC = \sum_i wi \ (MAC)i \quad (2)$$

The weight fraction of the ith constituent element is denoted by W_i. The HVL is the thickness of a sample that lowers the intensity of radiation by half. Furthermore, the MFP is the distance at which the function 1/e reduces the intensity of the radiation; these are essential shielding parameters. These are important shielding parameters [27– 29].

$$HVL = \frac{\ln(2)}{\mu} \quad (3)$$

$$TVL = \frac{\ln(10)}{\mu} \quad (4)$$

$$HVL = \frac{1}{\mu} \quad (5)$$

An effective atomic number (Z_{eff}) that varies with the material, as well as certain variables of the interacting radiation, provides material information, and the Z_{eff} values of the samples were included in this study [30]:

$$Zeff = \frac{\sum_i fiAi \ (MAC)i}{\sum_j fj \frac{Aj}{Zj} \ (MAC)j} \quad (6)$$

where f_j is the atomic weight and number of the i-th absorber element, and A_i and Z_i are the atomic weight and number of the i-th absorber element. As an example, consider the absorber material.

The ability to calculate the electron density N_{eff} value:

$$Neff = NA \frac{nZeff}{\sum_i niAi} \quad (7)$$

N_A denotes Avogadro's number, and n_i denotes the total number of elements in the sample.

3. RESULTS AND DISCUSSION

3.1. Mass attenuation coefficient (MAC) and linear attenuation coefficient (LAC)

The LAC (cm^{-1}) value denotes attenuation per unit length and is independent of material density; it is the first gamma-ray absorption parameter obtained. This is an important parameter. Figures 1(a) and (b) show the energy-dependent changes in LAC. Even though the LAC values of the samples studied appear to decrease with increased energy. LAC is 1.45297 cm^{-1} at 100 KeV. The variation in MAC values as a function of energy for MAC values calculated with the EpiXS programme sample is depicted in Figure 1, and the changes are related to photon energy. MAC values tend to decrease rapidly with energy at medium and low energies. This trend is explained by the change in the photoelectric interaction cross-section caused by the $Z^4/E^{3.5}$ relationship. Figure 1 depicts a sudden increase in energy from 30 KeV to 200 KeV. This sharp peak corresponds to the element's K-absorption edge. It is equivalent to the energy of the absorbed photon. Because of the linear change in Compton scattering with Z at intermediate energies, the MAC values for the sample are constants. The interaction mechanism of pair production (which varies with Z^2) caused the MAC values to rise once more at higher energies [31]. MAC values of the sample, it is clear that their low energy values vary dramatically. In this range, the photoelectric effect is very strong (E_{Photon} <100 keV). The absorption cross-section of a material varies according to the number of atoms in it (Z^{4-5}). Due to increased energy, the LAC and MAC values of the samples are rapidly decreasing. These high-energy photons penetrate deeper into materials, significantly reducing their ability to reduce radiation [32-33].

Based on the investigation and simulation of shielding parameters, the fabricated CuO nanomaterial demonstrates significant shielding properties against gamma radiation. The attenuation effectiveness is highly energy-dependent. At very low energy (5 KeV), driven predominantly by the Photoelectric Effect, the material exhibits maximum absorption, with a Linear Attenuation Coefficient (LAC) of 1002.13 cm^{-1} and a Mass Attenuation Coefficient (MAC) of 161.226 cm^2/g^{-1}. A sharp decrease in attenuation occurs as energy increases; for example, at 100 KeV, the LAC and MAC drop significantly to 1.45297 cm^{-1} and 0.39846 cm^2/g^{-1}, respectively. At 1 MeV (1000 KeV), the attenuation is considerably lower (LAC: 0.00260 cm^{-1}, MAC: 0.05987 cm^2/g^{-1}), reflecting the deeper penetration of high-energy photons. While attenuation remains low at high energies, the MAC values tend to rise again at the highest energies due to the dominant contribution of pair production, as shown in Table 1.

3.2. The tenth value layer values, the half value layer, and the mean free path

The HVL, TVL, and MFP are critical parameters for determining gamma shielding capacity and environmental gamma radiation levels. Figure 2 (a-c) shows that the MFP, TVL, and HVL values are generally very low at energies

© Ariston Publications 2025. All rights reserved.

up to 1000 keV, confirming the material's strong gamma shielding capability in this energy range [34-36]. As the photon energy increases, these values tend to increase (meaning the material becomes less effective). Low Energy (e.g., at 5 KeV). The values for MFP (0.00098 cm), HVL (≈6.813×10−4 cm), and TVL (≈0.00068 cm) are indeed extremely low. Low MFP, HVL, and TVL values signify that a material has superior shielding characteristics, as a smaller thickness is required to significantly reduce the radiation intensity. This high attenuation at low energies is primarily due to the dominance of the photoelectric effect. As the photon energy increases, the MFP, HVL, and TVL values increase significantly. For example, the HVL increases from 6.813×10^{-4} cm at 5 KeV to 3.79541 cm at 10000 KeV. The increase in HVL indicates that the penetrating ability of the photons increases with energy, thereby requiring a greater thickness of the material for effective attenuation. This correlates with the rapid decrease in LAC and MAC values at higher energies, where "high-energy photons penetrate deeper into materials, significantly reducing their ability to reduce radiation" [37-40]. The relationship between HVL and energy means "an increase in energy causes an increase in HVL". The data in Table 2 shows that the MFP, HVL, and TVL values generally peak around 9000 KeV to 11000 KeV (e.g., HVL ≈3.795 cm at 10000 KeV), and then slightly decrease toward 15000 KeV (HVL ≈3.705 cm).

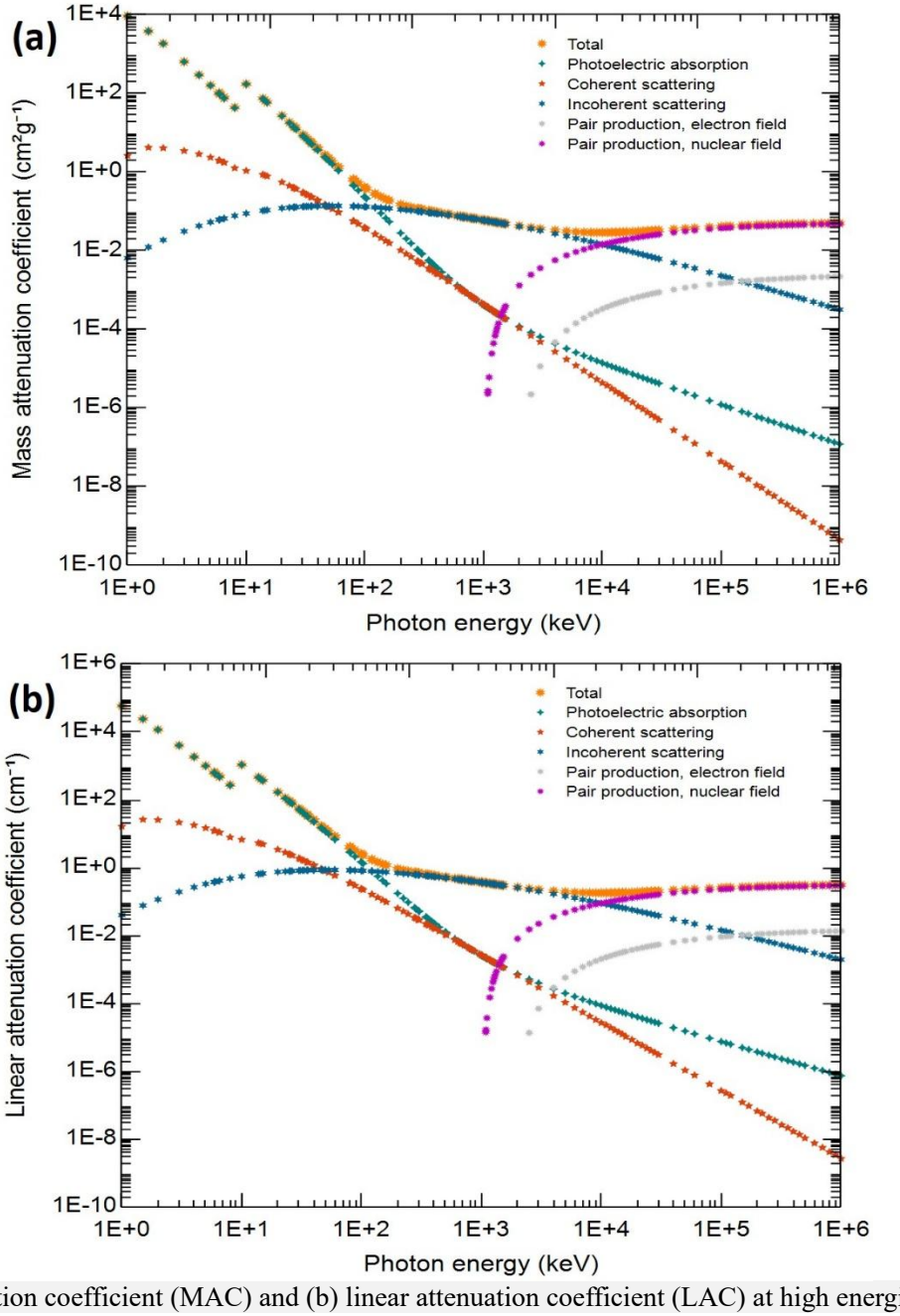

Fig. 1. (a) Mass attenuation coefficient (MAC) and (b) linear attenuation coefficient (LAC) at high energies for CuO.

 © Ariston Publications 2025. All rights reserved.

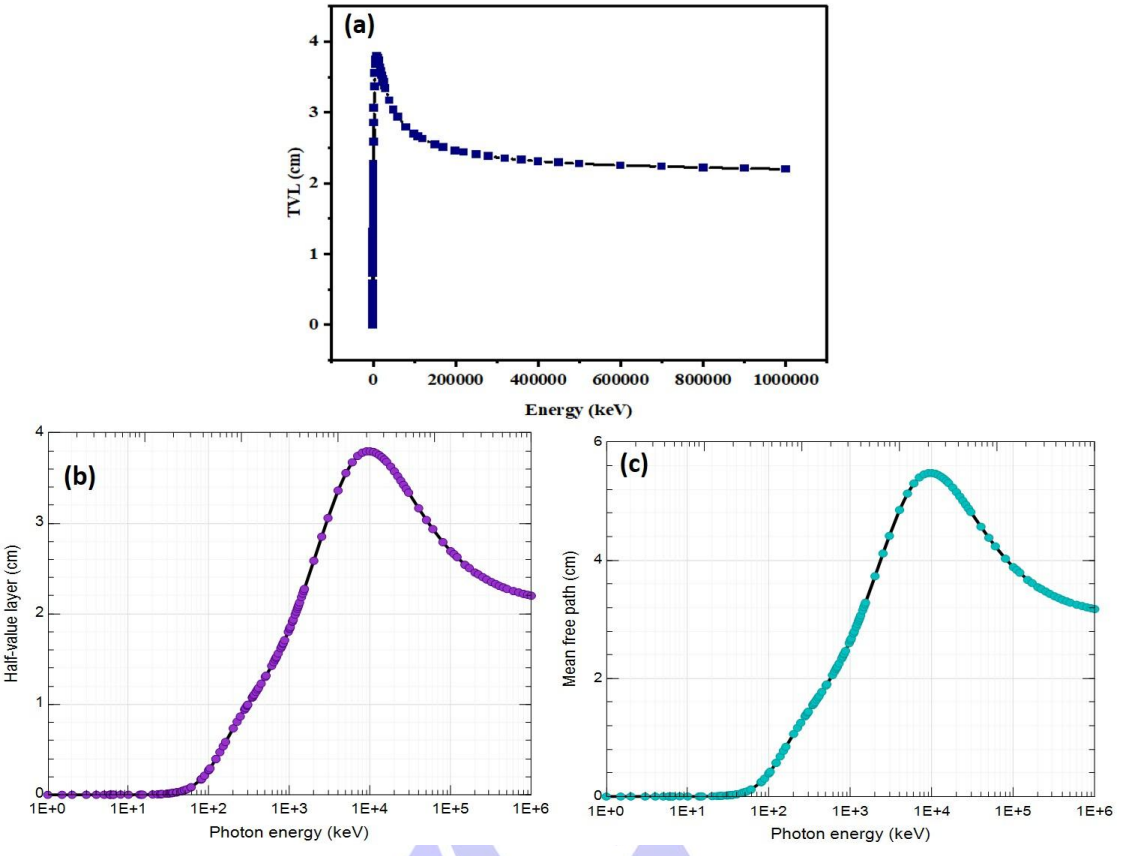

Fig. 2. (a) The tenth value layer (TVL) values, (b) the half value layer (HVL) values, and (c) mean free path (MFP) versus the incident photon energy of the sample *versus* the incident photon energy of the sample.

The MAC values are influenced by the interaction mechanisms, which include the photoelectric effect, Compton scattering, and pair production. The rise in MAC values (and corresponding slight decrease in HVL/MFP) at higher energies (>1022 KeV) is attributed to the interaction mechanism of pair production (which varies with Z2) becoming dominant. Specifically, for the highest energy range investigated (6000 KeV to 15000 KeV), the pair production process completely dominates, and the accumulation factors for deeper penetration depths increase due to Z^2. From the found result, CuO was found to have the best shielding characteristics, and this is supported by the extremely low MFP, TVL, and HVL values observed at low energies [41-44].

3.3. The effective atomic number (Z_{eff}) and electron density (N_{eff})

The effective atomic number, also known as the virtual atomic number, reflects the total of any material composed of more than one atom and implies that the shielding substance possesses the property [45-48].

Furthermore, this number characterizes materials in a set of material classes based on their shielding capacities and can be used to select the best-shielding material. This parameter is proportional to incident photon energy and is directly affected by material atom types. Compton scattering interactions affect it. Figure 3 depicts the viewpoint of the procured Z_{eff} for photon-energy-varying samples. A sample's ability to absorb radiation is indicated by the magnitude of its Z_{eff} value. Figure 3 depicts three photon-substance interaction procedures that influenced Z_{eff} values. Z_{eff}'s energy dependence decreased in the middle and high energy zones, with the lowest values observed in high energies, where pair production (change with log E) was dominant. The sample's Z_{eff} values ranged from 18 to 25.

Figure 3 depicts the variation in N_{eff} values as a function of incident photon energy. With energies up to 1 MeV, the results show a decreasing order of N_{eff} values. The MAC and Z_{eff} value systems produce significantly different results. The outcome can be related to the mole fraction and atomic mass of the material's constituent elements. The lower Neff's value. As a result of these findings, it is not possible to claim that a material has a higher shielding capacity regardless of whether its N_{eff} value is higher or lower. As a result, if a material includes elements with large atomic masses, the material's N_{eff} values will be low at any photon energy.

3.4. Cross section

© Ariston Publications 2025. All rights reserved.

The number of free electrons generated by photons entering the material is denoted by C_{eff}. This parameter is related to the materials' densities and effective electron densities. The three major photon-matter interactions can change the number of free electrons in a material. This modification may have an impact on the material's effective electron density and, as a result, effective conductivity (C_{eff}). As a result, variations in photon energy can influence C_{eff} values. As a result, changes in the C_{eff} value of a material can affect some of its properties, such as conductance. As a result, the C_{eff} values of the current sample were determined in this study.

Table 1. Mass attenuation coefficient (MAC) and linear attenuation coefficient (LAC) at high energies for CuO nanoparticles.

Energy (KeV)	LAC (cm^{-1})	MAC (cm^2/g^{-1})
5	1002.13	161.226
6	603.758	97.6817
8	269.181	43.9964
10	1086.75	173.386
15	370.241	59.5658
20	167.433	27.2018
30	52.8703	8.81071
40	22.8632	3.94803
50	11.803	2.13651
60	6.84047	1.31507
80	2.86728	0.64514
100	1.45297	0.39846
150	0.42183	0.20484
200	0.17637	0.14964
300	0.05311	0.11092
400	0.02359	0.09439
500	0.01299	0.08433
600	0.00819	0.07713
800	0.00418	0.06694
1000	0.00260	0.05987
1022	0.00249	0.05922
1250	0.00168	0.05342
1500	0.00120	0.04873
2000	0.00074	0.04248
3000	0.00040	0.03592
4000	0.00027	0.03267
5000	0.00020	0.03090
6000	0.000160	0.02990
7000	0.00013	0.02934
8000	0.000113	0.02906
9000	0.00010	0.02894
10000	0.00009	0.02894
11000	0.000078	0.02900
12000	0.000071	0.02912
13000	0.000065	0.02927
14000	0.000060	0.02945
15000	0.000055	0.02965

Figure 4 shows how these values change as incident photon energy increases. C_{eff} values are also proportional to N_{eff} values. Moreover, even though C_{eff} values are directly proportional to N_{eff} values, the ordering of C_{eff} values with energy differs from that of N_{eff} values due to sample density differences.

Table 2. The tenth value layer values, the half value layer values, mean free path (MFP).

Energy (KeV)	MFP (cm)	HVL (cm)	TVL (cm)
5	0.00098	0.00068	0.00068
6	0.00162	0.00112	0.00112
8	0.0036	0.0025	0.0025
10	0.00091	0.00063	0.00063
15	0.00266	0.00184	0.00184
20	0.00583	0.00404	0.00404
30	0.01799	0.01247	0.01247
40	0.04014	0.02782	0.02782
50	0.07418	0.05142	0.05142
60	0.12051	0.08353	0.08353
80	0.24565	0.17027	0.17027
100	0.39773	0.27569	0.27569
150	0.77368	0.53628	0.53628
200	1.05906	0.73408	0.73408
300	1.42875	0.99034	0.99034
400	1.67893	1.16375	1.16375
500	1.87934	1.30266	1.30266
600	2.05477	1.42426	1.42426
800	2.36746	1.641	1.641
1000	2.64687	1.83467	1.83467
1022	2.67619	1.855	1.855
1250	2.96656	2.05626	2.05626
1500	3.25211	2.25419	2.2542
2000	3.73065	2.58589	2.58589
3000	4.41193	3.05812	3.05812
4000	4.85036	3.36201	3.36202
5000	5.12896	3.55512	3.55513
6000	5.2998	3.67354	3.67355
7000	5.40209	3.74444	3.74443
8000	5.45419	3.78055	3.78056
9000	5.47568	3.79545	3.79545
10000	5.47562	3.79541	3.7954
11000	5.46563	3.78848	3.78848
12000	5.4428	3.77266	3.77266
13000	5.41378	3.75255	3.75254
14000	5.38136	3.73008	3.73007
15000	5.34534	3.70511	3.7051

Figure 4 shows how the ACS (atomic cross-section) and ECS (electronic cross-section) values change with increasing photon energy. As photon energy increases, the ACS values of the sample studied decrease, possibly due to reduced photon-atom interaction. Furthermore, as shown in Figure 4, sample exhibit a sharp decrease after 100 keV energy value.

© Ariston Publications 2025. All rights reserved.

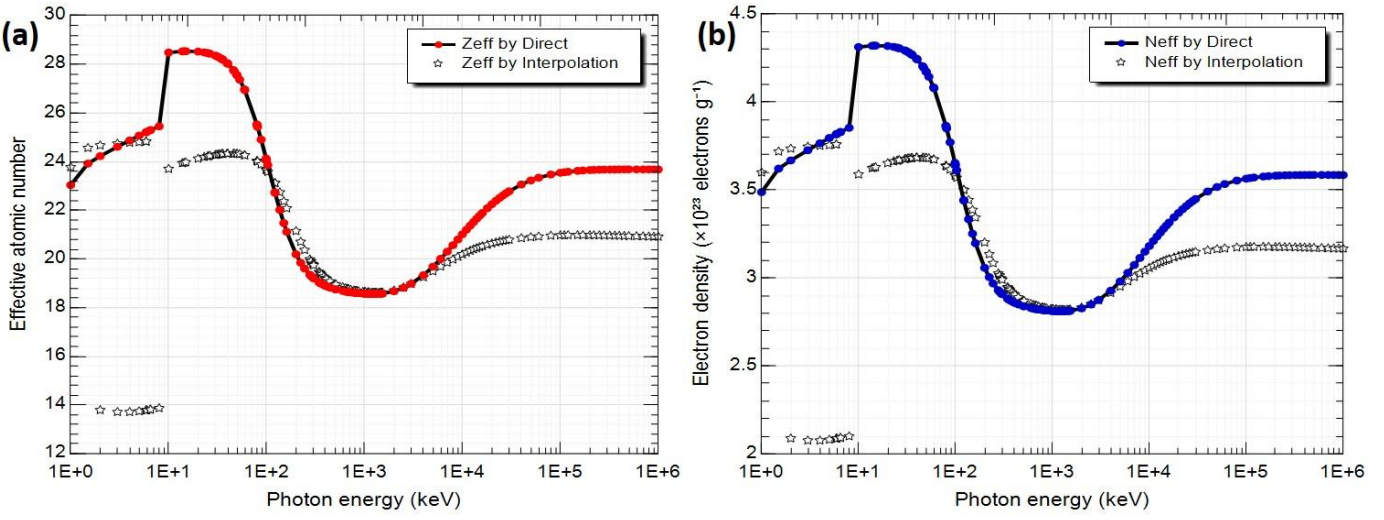

Fig. 3. The effective atomic number Z_{eff}, N_{eff}, and Z_{aq} values versus the incident photon energy of the samples.

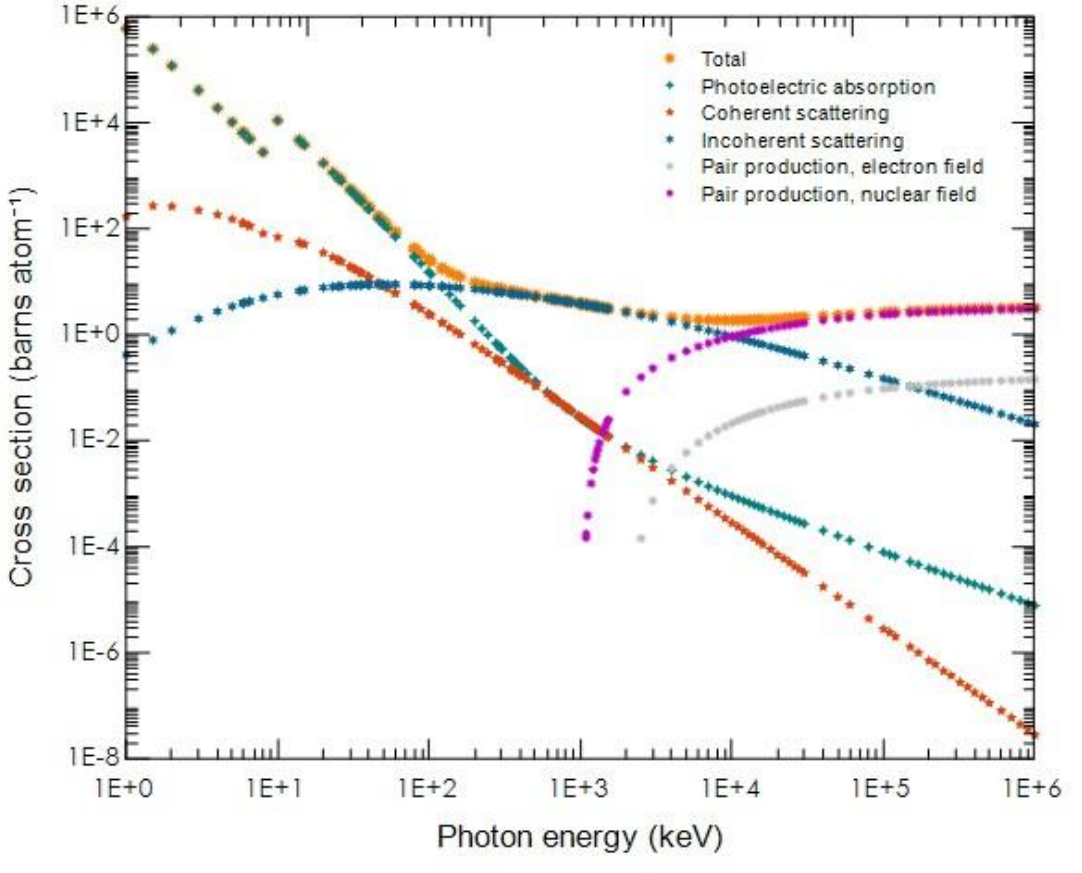

Fig. 4. Cross-section *versus* the incident photon energy of the sample.

3.5. Photon build-up factors

Photon build-up factors, which illustrate the possibility of photon scattering, are a further significant variable in radiation protection applications. The initial stage in the calculation is to determine how many photons are scattered from the total number of photons striking the material. R is a pure mathematical process calculated by dividing the total cross-sections by the incoherent scattering cross-sections at each energy value. To calculate the build-up factors, G-P fitting coefficients (a, b, c, d, and X_K), R, and Z_{eq} values have been supplied. Figure 5 shows variations in R values for

© Ariston Publications 2025. All rights reserved.

energies ranging from 15 to 15000 KeV. In the middle energy region, Compton scattering, also known as inelastic scattering, reigns supreme. When using a constant overall cross-section, the inelastic scattering cross-section reaches its maximum within the specified limits and becomes almost entirely independent of the material composition. Furthermore, as energy increases, pair production takes over, reducing the possibility of Compton scattering. As a result, after a certain maximum, R values tend to fall. When photons are absorbed by materials, the virtual atomic number that identifies the complex material is Z_{eff}; when scattering occurs, this value is Z_{eq}. Figure 5 depicts the changes in Z_{eq} values for the sample studied.

Figure 6 shows the G-P (Geometric Progression) fitting coefficients (a, b, c, d, and Xk) used to model or parameterize the EBF and EABF values. These coefficients allow for the easy calculation of buildup factors for various energies and depths without having to rely solely on the plotted curves. Buildup factors, the exposure buildup factors (EBF) and Energy absorption factor (EABF) are critical when constructing gamma radiation shielding and medical physics applications [32, 22].

In this study, Figure 5 also depicts how EBF values vary with depth of penetration at four different energy levels. The EBF values increase from 15 KeV to 2000KeV then decrease at high energy, indicating that scattered multiple times is extremely unlikely at these energies. As a result, irrespective of MFP, participation in EBF in extremely low-income areas may be overlooked. As energy increases at any MFP value, the changing photon-matter interaction mechanism changes to a decreasing or increasing order of sample. In addition, EBF participation in the high-energy region, particularly at high MFP values, should be considered. Different parameters including such photon energy absorption and dose were used to evaluate buildup factors. Energy values and penetration have an impact on EBF and EABF.

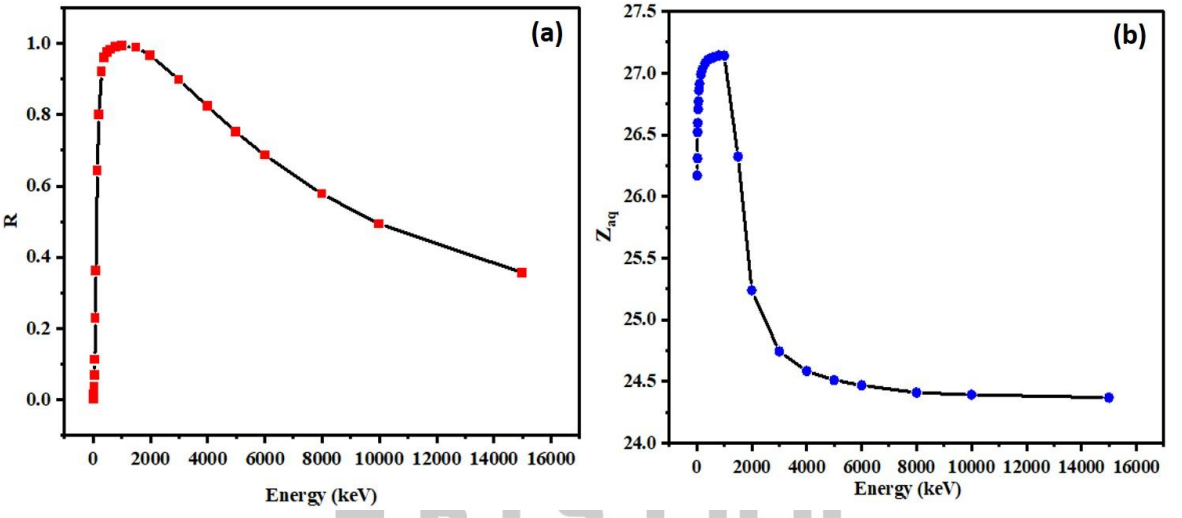

Fig. 5. (a) R values, (b) Z_{aq} versus the incident photon energy of the sample *versus* the incident photon energy of the sample.

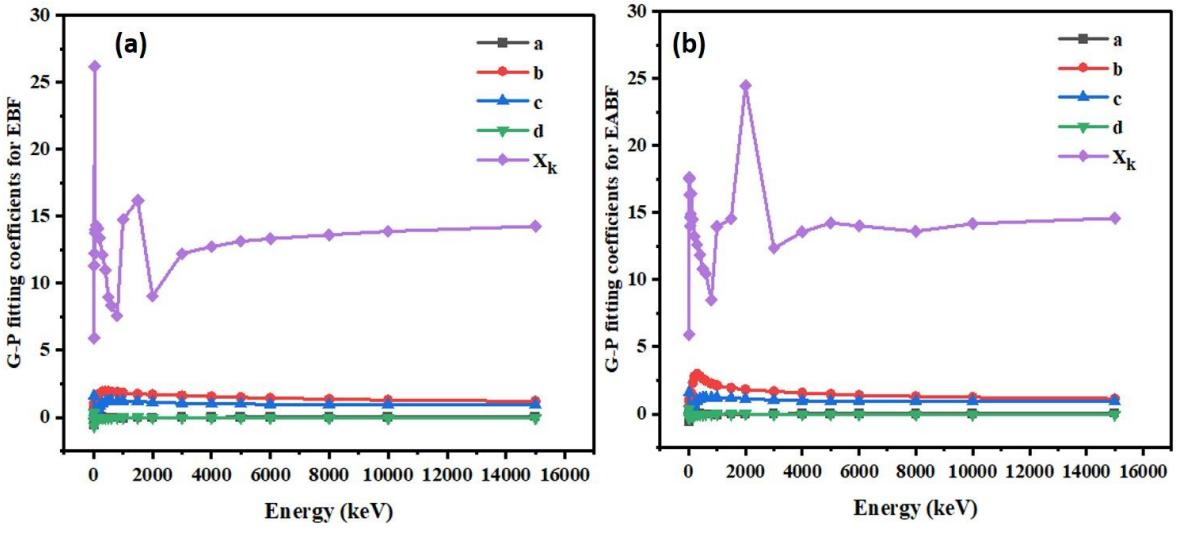

Fig. 6. G-P fitting coefficients (a, b, c, d, and XK) for EBF and EABF.

 © Ariston Publications 2025. All rights reserved.

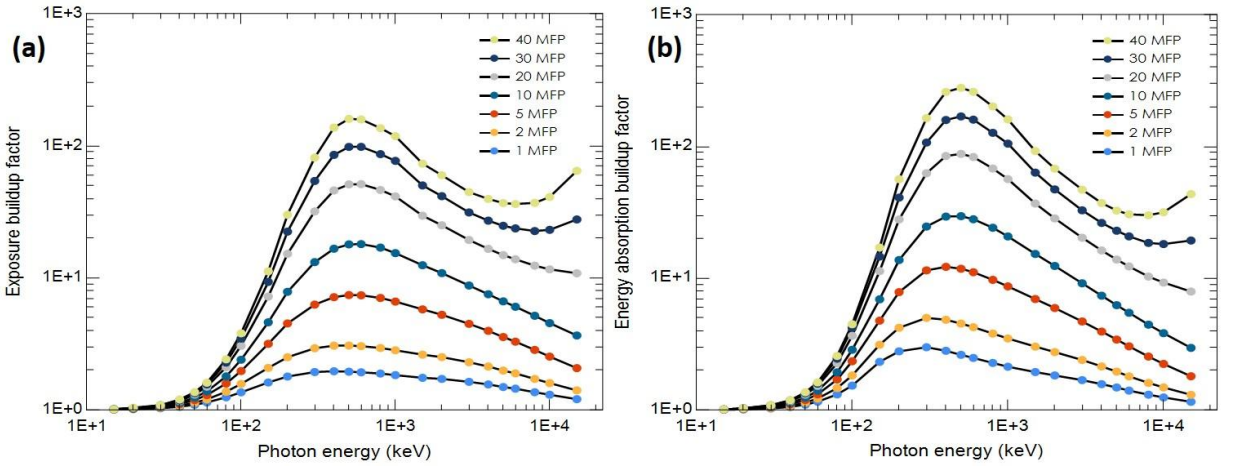

Fig. 7. The exposure buildup factors and Energy absorption factor, 30, 35, at 1, 2, 5, 10, 20, 30, and 40 mfp.

Figure 7 shows the depths of the investigated samples (1, 2, 5, 10, 20, 30, and 40 mfp). When Figure 7 are compared, it is clear that at medium energies where Compton scattering occurs, the EBF and EABF values of the samples change proportionally to Z_{eq} values. At energies greater than 3000 KeV, the pair production Process completely dominates. As Z_{eq} increases, the accumulation factors for deeper penetration depths (>15mfp) increase. These particles may escape or collide multiple times within the material after coming to rest at shallow penetration depths (15mfp). Secondary gamma rays help to strengthen primary gamma rays as a result, the sample reacted more strongly to gamma radiation. Because pair production is dominant in this energy range, the EBF and EABF values of the investigated samples increased more rapidly at 6000-15000 KeV due to Z^2. The EBF and EABF values increased as penetration depth increased as illustrated in Figure 7.

4. CONCLUSION

CuO nanoparticles were successfully synthesized via a simple and cost-effective coprecipitation method and evaluated for their gamma-ray shielding performance using the EpiXS computational approach. The results demonstrate that the shielding efficiency of CuO nanoparticles is strongly dependent on photon energy and the dominant interaction mechanisms. The material exhibits excellent attenuation capability at low photon energies, where the photoelectric effect prevails, as confirmed by high mass and linear attenuation coefficients and exceptionally low half-value layer and mean free path values. As photon energy increases, attenuation parameters decrease due to the dominance of Compton scattering, followed by a slight enhancement at higher energies attributed to pair production. The effective atomic number of CuO nanoparticles remains within a favorable range across the investigated energy spectrum, supporting efficient photon–matter interactions. Buildup factor analysis indicates that photon accumulation becomes significant at higher energies and greater penetration depths, which should be considered in practical shielding design. Overall, the synthesized CuO nanoparticles combine ease of fabrication, lightweight characteristics, and environmental friendliness with promising gamma-ray shielding performance, particularly in the low- and intermediate-energy regions. These findings highlight CuO nanomaterials as a viable alternative to conventional heavy and toxic shielding materials for radiation protection and medical physics applications.

DECLARATIONS

Ethical Approval

We affirm that this manuscript is an original work, has not been previously published, and is not currently under consideration for publication in any other journal or conference proceedings. All authors have reviewed and approved the manuscript, and the order of authorship has been mutually agreed upon.

Funding

Not applicable

Availability of data and material

The datasets used and/or analyzed during the current study are available from the corresponding author on reasonable request.

Conflicts of Interest

The authors declare that they have no financial or personal interests that could have influenced the research and findings presented in this paper. The authors alone are responsible for the content and writing of this article.

© Ariston Publications 2025. All rights reserved.

Authors' contributions

All authors contributed equally in the preparation of this manuscript.

REFERENCES

[1] Allam, E.A., El-Sharkawy, R.M., El-Taher, A., Shaaban, E.R., Massoud, E.E.S. and Mahmoud, M.E., **2022**. Enhancement and optimization of gamma radiation shielding by doped nano HgO into nanoscale bentonite. *Nuclear Engineering and Technology*, *54*(6), pp.2253-2261.

[2] Acevedo-Del-Castillo, A., Águila-Toledo, E., Maldonado-Magnere, S. and Aguilar-Bolados, H., **2021**. A brief review on the high-energy electromagnetic radiation-shielding materials based on polymer nanocomposites. *International journal of molecular sciences*, *22*(16), p.9079.

[3] Saddeek, Y.B., Shaaban, K.H.S., Elsaman, R., El-Taher, A. and Amer, T.Z., **2018**. Attenuation-density anomalous relationship of lead alkali borosilicate glasses. *Radiation Physics and Chemistry*, *150*, pp.182-188.

[4] Gungor, A., Akbay, I.K., Yasar, D. and Ozdemir, T., **2018**. Flexible X/gamma ray shielding composite material of EPDM rubber with bismuth trioxide: Mechanical, thermal investigations and attenuation tests. *Progress in Nuclear Energy*, *106*, pp.262-269.

[5] Lu, X., Zheng, Y., Yang, J. and Qu, J., **2020**. Multifunctional paraffin wax/carbon nanotube sponge composites with simultaneous high-efficient thermal management and electromagnetic interference shielding efficiencies for electronic devices. *Composites Part B: Engineering*, *199*, p.108308.

[6] Khalil, A., Bondouk, I.I., Allam, E.A., Nabil, I.M., Al-Abyad, M., Saudi, H., El-Taher, A., Mahmoud, M.E. and Amar, A., **2024**. A binary composite material of nano polyaniline intercalated with Nano-Fe2O3 for enhancing gamma-radiation-shielding properties: experimental and simulation study. *Progress in Nuclear Energy*, *169*, p.105067.

[7] Singh, C., Singh, T., Kumar, A. and Mudahar, G.S., **2004**. Energy and chemical composition dependence of mass attenuation coefficients of building materials. *Annals of nuclear Energy*, *31*(10), pp.1199-1205.

[8] Shirkhanloo, H., Safari, M., Amini, S.M. and Rashidi, M., **2017**. Novel semisolid design based on bismuth oxide (Bi2O3) nanoparticles for radiation protection. *Nanomedicine Research Journal*, *2*(4), pp.230-238.

[9] Mourad, M., Abdou, Y., Berber, M.R. and Elhussiny, F., **2021**. Using nano tungsten oxide polymer composite as a gamma radiation shielding. *Delta Journal of Science*, *43*(1), pp.126-132.

[10] Quarcoo, F., **2015**. *The use of low linear density polyethylene in the production of LLDPE-sand-stone composites* (Doctoral dissertation).

[11] El-Taher, A., Zakaly, H.M., Allam, E.A., El-Sharkawy, R.M., Al Meshari, M., Soliman, A.M., Salih, M., Alahmad, H. and Mahmoud, M.E., **2025**. Fluka and microshield simulation assessment of nuclear radiation attenuation by binary nanocomposites. *Radiation Physics and Chemistry*, *229*, p.112409.

[12] Rilwan, U., Abdulazeez, M.A., Maina, I., Olasoji, O.W., El-Taher, A., Alhindawy, I.G., Mahmoud, K.A., Sayyed, M.I., Elsafi, M., Rashad, M. and Maghrbi, Y., **2025**. The use of coconut shell ash as partial replacement of cement to improve the thermal properties of concrete and waste management sustainability in Nigeria and Africa, for radiation shielding application. *Scientific African*, *27*, p.e02578.

[13] Rilwan, U., Abdulazeez, M.A., Maina, I., Olasoji, O.W., Olukotun, S.F., El-Taher, A., Sayyed, M.I., GY, N.C., Ahmed, G.J., Adeyeba, O.A. and Marashdeh, M.W., **2025**. Gamma radiation shielding and thermal performance of concrete with coconut shell ash replacement. *NIPES-Journal of Science and Technology Research*, *7*(2), pp.254-262.

[14] Negm, H.H., El-Sharkawy, R.M., Abdeltwab, E., Mostafa, M., Mahmoud, M.E. and El-Taher, A., **2024**. Evaluation of shielding properties of a developed nanocomposite from intercalated attapulgite clay by Cd/Pb oxides nanoparticles. *Physica Scripta*, *99*(5), p.055956.

[15] Saleh, A., Sayyed, M.I., Kumar, A. and Mansour, F.E., **2024**. Synthesis and gamma-ray shielding efficiency of borosilicate glasses doped with zinc oxide: comparative study. *Silicon*, *16*(10), pp.4427-4435.

[16] Kaewjaeng, S., Boonyu, K., Kim, H.J., Kaewkhao, J. and Kothan, S., 2020, October. Study on radiation shielding properties of glass samples doped with holmium. In *AIP conference proceedings* (Vol. 2279, No. 1, p. 060005). AIP Publishing LLC.

 © Ariston Publications 2025. All rights reserved.

[17] Naseer, K.A., Marimuthu, K., Mahmoud, K.A. and Sayyed, M.I., 2021. Impact of Bi2O3 modifier concentration on barium–zincborate glasses: physical, structural, elastic, and radiation-shielding properties. *The European Physical Journal Plus*, *136*(1), p.116.

[18] Kavaz, E., El_Agawany, F.I., Tekin, H.O., Perişanoğlu, U.F.U.K. and Rammah, Y.S., **2020**. Nuclear radiation shielding using barium borosilicate glass ceramics. *Journal of Physics and Chemistry of Solids*, *142*, p.109437.

[19] Singh, N., Singh, K.J., Singh, K. and Singh, H., **2004**. Comparative study of lead borate and bismuth lead borate glass systems as gamma-radiation shielding materials. *Nuclear Instruments and Methods in Physics Research Section B: Beam Interactions with Materials and Atoms*, *225*(3), pp.305-309.

[20] Mahmoud, M.E., El-Sharkawy, R.M., Allam, E.A., Elsaman, R. and El-Taher, A., **2019**. Fabrication and characterization of phosphotungstic acid-Copper oxide nanoparticles-Plastic waste nanocomposites for enhanced radiation-shielding. *Journal of Alloys and Compounds*, *803*, pp.768-777.

[21] El-Sharkawy, R.M., Allam, E.A., El-Taher, A., Elsaman, R., Massoud, E.E.S. and Mahmoud, M.E., **2022**. Synergistic effects on gamma-ray shielding by novel light-weight nanocomposite materials of bentonite containing nano Bi2O3 additive. *Ceramics International*, *48*(5), pp.7291-7303.

[22] El-Taher, A., Zakaly, H.M., El-Sharkawy, R., Allam, E.A., Al Meshari, M. and Mahmoud, M.E., **2023**. Effect of bismuth oxide nanoparticles on the radiation shielding of bentonite clay using Fluka modeling calculations and simulation studying. *Progress in Nuclear Energy*, *155*, p.104494.

[23] Hila, F.C., Asuncion-Astronomo, A., Dingle, C.A.M., Jecong, J.F.M., Javier-Hila, A.M.V., Gili, M.B.Z., Balderas, C.V., Lopez, G.E.P., Guillermo, N.R.D. and Amorsolo Jr, A.V., **2021**. EpiXS: A Windows-based program for photon attenuation, dosimetry and shielding based on EPICS2017 (ENDF/B-VIII) and EPDL97 (ENDF/B-VI. 8). *Radiation Physics and Chemistry*, *182*, p.109331.

[24] Abdelhamid, M., Fouad, D., Alian, A., Nasr, A.A., Abd-Allah, H., Farouk, M., Abd Elmaleck, B.S., Alexiou, A., Papadakis, M., Batiha, G.E.S. and Anwar, F.A., **2025**. Evaluating the In Vitro Anthelmintic Activity of Zinc Oxide Nanoparticles (ZnO-NPs) Against the Adult Stages of Fasciola hepatica. *Veterinary Medicine and Science*, *11*(1), p.e70170.

[25] El-Taher, A., Ali, A.M., Saddeek, Y.B., Elsaman, R., Algarni, H., Shaaban, K. and Amer, T.Z., **2019**. Gamma ray shielding and structural properties of iron alkali alumino-phosphate glasses modified by PbO. *Radiation Physics and Chemistry*, *165*, p.108403.

[26] Yue, K., Luo, W., Dong, X., Wang, C., Wu, G., Jiang, M. and Zha, Y., **2009**. A new lead-free radiation shielding material for radiotherapy. *Radiation protection dosimetry*, *133*(4), pp.256-260.

[27] Ivanova, T., Bliznakova, K. and Pallikarakis, N., **2006**. Simulation studies of field shaping in rotational radiation therapy. *Medical physics*, *33*(11), pp.4289-4298.

[28] El-Sharkawy, R.M., Shaaban, K.S., Elsaman, R., Allam, E.A., El-Taher, A. and Mahmoud, M.E., **2020**. Investigation of mechanical and radiation shielding characteristics of novel glass systems with the composition xNiO-20ZnO-60B2O3-(20-x) CdO based on nanometal oxides. *Journal of Non-Crystalline Solids*, *528*, p.119754.

[29] El-Taher, A., Zakaly, H.M., Pyshkina, M., Allam, E.A., El-Sharkawy, R.M., Mahmoud, M.E. and Abdel-Rahman, M.A., **2021**. A comparative study between fluka and microshield modeling calculations to study the radiation-shielding of nanoparticles and plastic waste composites. *Zeitschrift für anorganische und allgemeine Chemie*, *647*(10), pp.1083-1090.

[30] El-Sharkawy, R.M., Allam, E.A., El-Taher, A., Shaaban, E.R. and Mahmoud, M.E., **2021**. Synergistic effect of nano-bentonite and nanocadmium oxide doping concentrations on assembly, characterization, and enhanced gamma-rays shielding properties of polypropylene ternary nanocomposites. *International Journal of Energy Research*, *45*(6), pp.8942-8959.

[31] El-Taher, A., Mahmoud, H.M. and Abbady, A.G., **2007**. Comparative study of attenuation and scattering of gamma-rays through two intermediate rocks. *Indian Journal of Pure and Applied Physics*, *45*(3), pp.198-203.

[32] Allam, E.A., El-Sharkawy, R.M., Shaaban, K.S., El-Taher, A., Mahmoud, M.E. and El Sayed, Y., **2022**. Structural and thermal properties of nickel oxide nanoparticles doped cadmium zinc borate glasses: preparation and characterization. *Digest Journal of Nanomaterials & Biostructures (DJNB)*, *17*(1).

[33] Shan, F.K., Liu, Z.F., Liu, G.X., Lee, W.J., Lee, G.H., Kim, I.S., Shin, B.C. and Yu, Y.S., **2004**. Aging and annealing effects of ZnO thin films on GaAs substrates

© Ariston Publications 2025. All rights reserved.

deposited by pulsed laser deposition. *Journal of electroceramics*, *13*(1), pp.195-200.

[34] Negm, H., Abd-Allah, H., Abdel-Latief, A.Y., Abdel-Rahim, M.A., El-Taher, A. and Shaalan, N.M., **2024**. Fabrication and characterization of structured Zn1-xCdxWO4 (0≤ x≤ 1) with tunable photoluminescent and promising applicable heterometallic nanocomposites in shielding properties. *Radiation Physics and Chemistry*, *215*, p.111335.

[35] Bhuyan, T., Mishra, K., Khanuja, M., Prasad, R. and Varma, A., **2015**. Biosynthesis of zinc oxide nanoparticles from Azadirachta indica for antibacterial and photocatalytic applications. *Materials Science in Semiconductor Processing*, *32*, pp.55-61.

[36] Jones, C.G., **2005**. A review of the history of US radiation protection regulations, recommendations, and standards. *Health physics*, *88*(2), pp.105-124.

[37] Zakaly, H.M., Ashry, A., El-Taher, A., Abbady, A.G., Allam, E.A., El-Sharkawy, R.M. and Mahmoud, M.E., **2021**. Role of novel ternary nanocomposites polypropylene in nuclear radiation attenuation properties: In-depth simulation study. *Radiation Physics and Chemistry*, *188*, p.109667.

[38] Alafer, F., Sallam, F.H., Al Meshari, M., Alzamil, Y., Abanomy, A., Alhujaili, S. and El-Taher, A., **2024**. The influence of thermal treatment on the structural properties and gamma rays shielding of bentonite clay ceramic. *Radiation Physics and Chemistry*, *217*, p.111531.

[39] Rilwan, U., Aliyu, G.M., Olukotun, S.F., Idris, M.M., Mundi, A.A., Bello, S., Umar, I., El-Taher, A. and Mahmoud, K.A., **2024**. Recycling and characterization of bone incorporated with concrete for gamma-radiation shielding applications. *Nuclear Engineering and Technology*, *56*(7), pp.2828-2834.

[40] Negm, H.H., Allam, E.A., Abdeltwab, E., Mostafa, M., Mahmoud, M.E. and El-Taher, A., **2024**. A new nanocomposite of copper oxide and magnetite intercalated into Attapulgite clay to enhance the radiation shielding. *Radiation Physics and Chemistry*, *216*, p.111398.

[41] Rilwan, U., Edeh, S.A., Idris, M.M., Fatima, I.I., Olukotun, S.F., Arinseh, G.Z., Bonat, P.Z., El-Taher, A., Mahmoud, K.A., Hanafy, T.A. and Sayyed, M.I., **2025**. Influence of waste glass on the gamma-ray shielding performance of concrete. *Annals of Nuclear Energy*, *210*, p.110876.

[42] Negm, H.H., Allam, E.A., Nabil, I.M., Abdeltwab, E., Mostafa, M. and El-Taher, A., **2024**. Exploring the potential of attapulgite clay composites containing intercalated nano-cadmium oxide and nano-nickel oxide for efficient radiation shielding applications. *Radiation Physics and Chemistry*, *225*, p.112149.

[43] Almeshari, M., Sallam, F.H., Tharwat, M., Alzamil, Y., Salih, M., Alshoumr, B., Alyahyawi, A. and El-Taher, A., **2024**. Preparation and structure investigation of polyethylene terephthalate polyester reinforced Ni0. 5Zn0. 5Fe_2O_4 nanoparticles for gamma ray shielding performance. *Physica Scripta*, *99*(5), p.055311.

[44] Abuzaid, M.M., Susoy, G., Issa, S.A., Elshami, W., Kilicoglu, O. and Tekin, H.O., **2020**. Relationship between melting-conditions and gamma shielding performance of fluoro-sulfo-phosphate (FPS) glass systems: a comparative investigation. *Ceramics International*, *46*(10), pp.15255-15269.

[45] Mann, H.S., Brar, G.S. and Mudahar, G.S., **2016**. Gamma-ray shielding effectiveness of novel light-weight clay-flyash bricks. *Radiation Physics and Chemistry*, *127*, pp.97-101.

[46] Tekin, H.O., ALMisned, G., Rammah, Y.S., Ahmed, E.M., Ali, F.T., Baykal, D.S., Elshami, W., Zakaly, H.M., Issa, S.A., Kilic, G.Ö.K.H.A.N. and Ene, A., **2022**. Transmission factors, mechanical, and gamma ray attenuation properties of barium-phosphate-tungsten glasses: Incorporation impact of WO3. *Optik*, *267*, p.169643.

[47] Kumar, A., **2017**. Gamma ray shielding properties of PbO-Li2O-B2O3 glasses. *Radiation Physics and Chemistry*, *136*, pp.50-53.

[48] Davies, U., Kunchev, T., Cosgrove, P., Read, N., Kowalski, M.A. and Shwageraus, E., **2019**. Nuclear energy: Between global electricity demand, worldwide decarbonisation imperativeness, and planetary environmental implications. *Journal of Environmental Management*, *249*, pp.109208-109208.

 © Ariston Publications 2025. All rights reserved.